Evolution of Chemical Conditions and Estimated Plutonium Solubility in the Residual Waste Layer During Post-Closure Aging of Tank 18

Miles Denham

February 2012

Savannah River National Laboratory
Savannah River Nuclear Solutions
Aiken, SC 29808

Prepared for the U.S. Department of Energy Under Contract Number DE-AC09-08SR22470

SRNL
SAVANNAH RIVER NATIONAL LABORATORY

DISCLAIMER

Printed in the United States of America

Prepared for
U.S. Department of Energy

REVIEWS AND APPROVALS

AUTHOR:

_____

M. E. Denham, Environmental Restoration Technologies Date

TECHNICAL REVIEW:

_____

S. H. Reboul, Process Technology Programs Date

_____

D. T. Hobbs, Separation & Actinide Science Programs Date

APPROVAL:

_____

R. S. Aylward Date

Environmental Management

_____

H. H. Burns Date

Environmental & Chemical Process Technology Research Programs

_____

S. L. Marra Date

Environmental Management

_____

K. H. Rosenberger Date

SRR Closure and Disposal Assessment

Executive Summary

This document updates the Eh-pH transitions from grout aging simulations and the plutonium waste release model of Denham (2007, Rev. 1) based on new data. New thermodynamic data for cementitious minerals are used for the grout simulations. Newer thermodynamic data, recommended by plutonium experts (Plutonium Solubility Peer Review Report, LA-UR-12-00079), are used to estimate solubilities of plutonium at various pore water compositions expected during grout aging. In addition, a new grout formula is used in the grout aging simulations and apparent solubilities of coprecipitated plutonium are estimated using data from analysis of Tank 18 residual waste.

The conceptual model of waste release and the grout aging simulations are done in a manner similar to that of Denham (2007, Rev. 1). It is assumed that the pore fluid composition passing from the tank grout into the residual waste layer controls the solubility, and hence the waste release concentration of plutonium. Pore volumes of infiltrating fluid of an assumed composition are reacted with a hypothetical grout block using The Geochemist's Workbench® and changes in pore fluid chemistry correspond to the number of pore fluid volumes reacted. As in the earlier document, this results in three states of grout pore fluid composition throughout the simulation period that are termed Reduced Region II, Oxidized Region II, and Oxidized Region III. The one major difference from the earlier document is that pyrite is used to account for reducing capacity of the tank grout rather than pyrrhotite. This poises Eh at -0.47 volts during Reduced Region II. The major transitions in pore fluid composition are shown below:

Chemical Condition	Pore Volumes Reacted	Eh (volts)	pH	Total Carbonate (molar)
Reduced Region II	1 to 523	-0.47	11.1	6.7E-7
Oxidized Region II	524 to 2119	+0.56	11.1	6.9E-7
Oxidized Region III	>2119	+0.68	9.2	7.5E-5

Plutonium solubilities are estimated for discrete $PuO_{2(am,hyd)}$ particles and for plutonium coprecipitated with iron phases in the residual waste. Thermodynamic data for plutonium from the Nuclear Energy Agency are used to estimate the solubilities of the discrete particles for the three stages of pore fluid evolution. In Denham (2007, Rev. 1), the solubilities in the oxidized regions were estimated at Eh values in equilibrium with dissolved oxygen. Here, these are considered to be maximum possible solubilities because Eh values are unlikely to be in equilibrium with dissolved oxygen. More realistic Eh values are estimated here and plutonium solubilities calculated at these are considered more realistic. Apparent solubilities of plutonium that coprecipitated with iron phases are estimated from Pu:Fe ratios in Tank 18 residual waste

and the solubilities of the host iron phases. The estimated plutonium solubilities are shown below:

Grout Aging Region	$PuO_{2(am,hyd)}$ Max[a] (moles/liter)	$PuO_{2(am,hyd)}$ More Realistic[b] (moles/liter)	Coprecipitated (moles/liter)
Reduced Region II	3.2E-11	3.2E-11	3.0E-14
Oxidized Region II	5.2E-8	3.2E-11	2.5E-13
Oxidized Region III	7.8E-8	3.2E-11	5.0E-15

a—Eh values in equilibrium with dissolved oxygen

b—more realistic Eh values (explained in text)

Uncertainties in the grout simulations and plutonium solubility estimates are discussed. The primary uncertainty in the grout simulations is that little is known about the physical state of the grout as it ages. The simulations done here are pertinent to a porous medium, which may or may not be applicable to fractured grout, depending on the degree and nature of the fractures. Other uncertainties that are considered are the assumptions about the reducing capacity imparted by blast furnace slag, the effects of varying dissolved carbon dioxide and oxygen concentrations, and the treatment of silica in the simulations. The primary uncertainty in the estimates of plutonium solubility is that little is known about the exact form of plutonium in the residual waste. Other uncertainties include those inherent in the thermodynamic data, pH variations from those estimated in the grout simulations, the effects of the treatment of silica in the grout simulations, and the effect of varying total dissolved carbonate concentrations.

Contents

List of Tables

List of Figures

Objective

The objective of this document is to update the model for solubility controls on release of plutonium from residual waste in closed F-Area waste tanks. The update is based on new information including a new proposed grout formulation, chemical analysis of Tank 18 samples and more current thermodynamic data for plutonium and grout minerals. In addition, minor changes to the modeling of the grout chemical evolution have been made. It should be noted that the intent is to provide bounding solubilities for plutonium to be used in Performance Assessment modeling rather than trying to identify an exact concentration of plutonium in pore fluids released from a tank at any given time. This document also considers suggestions and opportunities for improvement regarding the plutonium modeling assumptions from the Plutonium Solubility Peer Review Report, LA-UR-12-00079.

Estimated Chemical Evolution of Reducing Grout

The conceptual model for chemical evolution of pore fluids in the tank grout remains essentially the same as that presented in Denham (2007, Rev. 1). Water infiltrating through the cover system enters the grout, reacts with grout minerals, and ultimately passes through the residual waste layer beneath the grout. As reactions in the grout progress and minerals dissolve or precipitate, the pore water chemistry exiting the grout changes. The changing pore water chemistry passing through the residual waste layer results in varying solubility of plutonium (Figure 1).

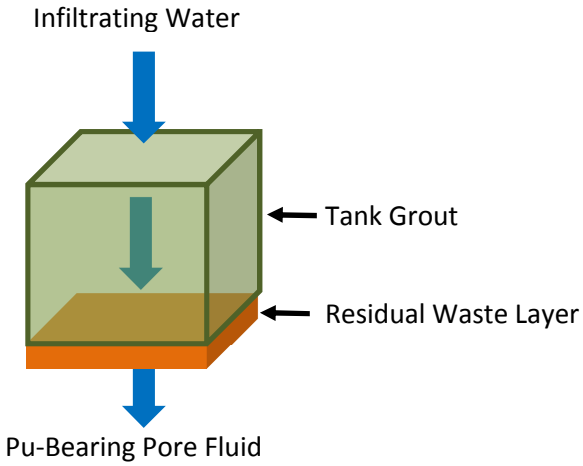

Figure 1: Conceptual model of pore fluid evolution and plutonium dissolution from the residual waste layer.

The simulation treats the tank grout as a porous medium. It is recognized that fracturing leads to heterogeneous flow patterns and that "fast" flow paths can occur within the tank. Yet, there is very little knowledge about the nature and effects of fracturing as the tank ages. In particular, the extent to which water passing through fractures interacts with the grout and, importantly, how water that reaches the residual layer through a fracture interacts with that layer. In the absence of such knowledge, this simulation treats the system as a porous medium with homogenous flow.

The bounding effect of fractures and fast-flow paths is addressed in sensitivity analyses within the Performance Assessment.

The Geochemist's Workbench® (Bethke, 2005) was used to simulate the major changes in pore fluid chemistry by modeling infiltrating fluid passing through a hypothetical 1 cubic meter block of tank grout. The simulations were done in the "Flush" mode so that each pore volume of fluid that enters the grout block completely replaces the previous reacted pore volume of fluid. This results in a reaction path model in which each pore volume of reacting fluid changes the mineralogy of the grout. The changes are reflected in the chemical composition of the fluid exiting the grout. The nature of this type of modeling produces step changes in the major chemical parameters of interest such as Eh and pH. These occur when a mineral that exerts the dominant control on a parameter is completely dissolved from the grout. Minor changes in these parameters may occur when a previously stable mineral begins to dissolve or a mineral begins to precipitate.

The initial mineralogy of the hypothetical grout block was estimated from the proposed grout formulation using a normative calculation. The normative mineralogy is simply a way to assign the chemical components of the bulk composition of the grout to mineral phases. The actual mineralogy is unknown so representative phases used in published cement simulations (e.g., Höglund, 2001; Lothenbach and Winnefeld, 2006) were chosen for the normative mineralogy. The grout formulation was from Stefanko and Langton (2011) and is shown in Table 1. Chemical analyses of each of the major cementitious constituents in the formulation were taken from Langton (2009, Attachment 2). These are shown in Table 2 along with the calculated bulk composition of the proposed grout.

Table 1: Proposed Tank 18 grout formulation (Stefanko and Langton, 2011).

Grout Component	Pounds Per Cubic Yard
Cement Type I/II	125
Slag Grade 100	210
Fly Ash Class F	363
Quartz Sand	1790
Gravel No. 8	800
Water	405

Table 2: Chemical compositions of major grout constituents (Langton, 2009) and bulk composition of proposed grout.

Component	Cement Type I/II (Wt.%)	Slag Grade 100 (Wt.%)	Fly Ash Class F (Wt.%)	Proposed Grout (g/m^3)
Al2O3	4.91	10.1	28.4	77388
CaO	64.3	35.8	1.41	95326
Fe2O3	3.5	0.36	7.99	20252
K2O	0.37	0.27	2.99	7050
MgO	0.95	12.6	1.0	18557
Na2O	0.09	0.22	0.44	1288
SO3	2.64	1.99	0.1	4653
SiO2	21.0	39.1	53.1	178647

The normative mineralogy of the grout was calculated by assigning major chemical components to cementitious minerals (Appendix 1 shows chemical formulas of all minerals considered):

- All SO_3 was assigned to gypsum with the requisite CaO
- All remaining CaO was assigned to JenH with the requisite SiO_2
- All MgO was assigned to OH-Hydrotalcite with the requisite Al_2O_3
- All remaining Al_2O_3 was assigned to gibbsite
- All Fe_2O_3 into was assigned to magnetite
- All remaining SiO_2 was assigned to amorphous silica

The alkalis were assumed to remain in the pore fluid to be leached out with the first pore volume of infiltrating fluid.

The normative mineralogy is shown in Table 3. The normative mineralogy is assumed to be completely hydrated because of the time lag between closure and breaching of the liner. Amorphous silica in the mineralogy represents the silica glass associated with blast furnace slag and fly ash. There is an excess of silica relative to portlandite, and thus all portlandite is assumed to react to the C-S-H phase JenH (Kulik, 2011). Iron likely exists in several phases, but magnetite was chosen here because it is a common phase in fly ash (e.g., Hower et al., 1999) and the Portland cement has a measured reduction capacity. Nevertheless, only 1 gram of magnetite was put in the "Basis" mineralogy for the grout simulations so that only reduction capacity from the slag would be considered. Pyrite was assigned to account for this because pyrrhotite, which has been observed in various types of slag quickly oxidizes to pyrite during grout simulations (Denham, 2007, Rev. 1).

Table 3: Calculated normative mineralogy of proposed grout and the equilibrium mineralogy as recalculated by The Geochemist's Workbench.

Minerals in System	Normative Mineralogy (g/m^3)	Recalculated (g/m^3)
Calcite	--	0.282
Ettringite	--	2.581E4
Gibbsite	1.005E5	9.724E4
Gypsum	1.001E4	--
JenH	2.145E5	9.688E4
TobD	--	1.210E5
Magnetite	1.958E4*	1.036
OH-Hydrotalcite	5.104E4	5.104E4
SiO2	1.049E5*	--
Pyrite	816	815.9
Inert	1536622	1536622

*Not used in base case simulation – see uncertainty section

When setting up a simulation in The Geochemist's Workbench® the normative mineralogy and pore fluid are entered into the "basis". From this starting point, The Geochemist's Workbench® recalculates the basis so that the fluid and minerals are in equilibrium. This may involve precipitation or dissolution of minerals. In the recalculated mineralogy in Table 3, a small amount of calcite and larger amounts of ettringite and TobD were added at the expense of carbonate in the original pore fluid and minerals containing calcium, aluminum, and silica.

Pyrite was included in the mineralogy to account for the reducing capacity of the grout. The reducing capacity of the grout was calculated from the amount of slag in the formulation and the measured reducing capacity of slag (Roberts and Kaplan, 2009). This was done as shown in Figure 2. Other iron was left out of the mineralogy with the exception of 1 gram of magnetite to hold a place for iron in the basis.

Calculation of Amount of Pyrite (accounts for reducing capacity of slag)

Measured reducing capacity of slag = 819 ueq/g (SRNL-STI-2009-00637 (Roberts and Kaplan, 2009))

Pyrite oxidation reaction: $FeS_2 + 3.75O_2 + 0.5H2O = Fe^{+3} + 2SO_4^{-2} + H^+$

15 moles electrons exchanged/mole pyrite oxidized MWpyrite=119.967 g/mole

15/119.967 = 0.125 moles electrons exchanged/gram pyrite oxidized

reduction capacity of pyrite = 125,000 ueq/gram

124,591 grams slag/m^3 of reducing grout

total reduction capacity= 124,591 g slag/m^3 grout x 819 ueq/ g slag = 1.02E8 ueq/m^3 grout

total reduction capacity expressed as grams pyrite = 1.02E8 ueq/m^3 grout ÷ 1.25E5 ueq/gram pyrite = 816 grams pyrite/m^3 grout

Figure 2: Details of calculation of amount of pyrite in grout mineralogy to account for reducing capacity imparted by the blast furnace slag.

The chemical composition of the infiltrating water that was reacted with the tank grout is shown in Table 4. It was derived by equilibrating an average rainwater composition (Strom and Kaback, 1992) with kaolinite and amorphous silica using The Geochemist's Workbench®. This was used to simulate rainwater that had passed through soil and the closure cap. The dissolved oxygen and carbon dioxide concentrations were calculated by equilibrating this water with atmospheric oxygen and carbon dioxide. It is assumed here that the pore water composition remains constant throughout the grout aging simulation. At some point, perhaps within the modeling period, the infiltration would revert to the composition of rainwater. Assuming rainwater composition in the future is similar to the composition from Strom and Kaback (1992), the primary difference would be lower dissolved aluminum and silica concentrations. The rainwater composition used here has a pH of 4.63 rather than 4.68, and the dissolved gas concentrations would be the same. Reaction of the infiltrating water with grout was closed with respect to atmospheric gases. A porosity of 21% (Stefanko and Langton, 2011) defined the pore volume of the grout block.

Table 4 : Infiltrating water composition used in grout evolution simulations.

Constituent	Concentration
pH	4.68
$O_{2(aq)}$	2.19E-4 moles/liter
$CO_{2(aq)}$	1.07E-5 moles/liter
Cl^-	2.74E-5 moles/liter
Na^+	8.69E-6 moles/liter
Ca^{+2}	2.06E-6 moles/liter
Mg^{+2}	1.34E-6 moles/liter
Al^{+3}	8.43E-7 moles/liter
$H_4SiO_{4(aq)}$	1.90E-3 moles/liter
SO_4^{-2}	1.35E-5 moles/liter

The simulations of the chemical evolution of tank grout were run using The Geochemist's Workbench® in a manner similar to Denham (2007, Rev. 1), with some notable exceptions. The current simulations used a different set of cementitious minerals with different thermodynamic data obtained from Lothenbach and Winnefeld (2006) and Kulik (2011). The PHREEQC thermodynamic database (provided with The Geochemist's Workbench® as "thermo_phreeqc") was used as the framework to build a thermodynamic database suitable for simulations of cementitious materials. In addition to cementitious minerals, the thermodynamic data for the iron minerals pyrite, magnetite, and maghemite were updated. A brief summary of the various sources of thermodynamic data used in this report appears in Appendix 2. The minerals allowed in the simulations are shown in Table 5 and the thermodynamic data are presented in Appendix 2.

Table 5: Minerals allowed in simulations of tank grout chemical evolution.

Brucite	Gibbsite	Monocarboaluminate
C4AH13	Gypsum	OH-Hydrotalcite
Calcite	JenD	Portlandite
Ettringite	JenH	SiO2(am)
Fe(OH)3(am)	Maghemite	TobD
Fe-Ettringite	Magnetite	TobH

It should be noted that an inherent assumption in these simulations is that the minerals that make up the residual waste layer do not strongly influence the composition of the pore fluids. Hay (2012) has observed gibbsite, hematite, cejkaite, calcite, a nitrated sodium aluminum silicate, and a uranyl hydrogen fluoride hydrate in Tank 18 residual waste. The hematite is assumed here to convert to magnetite prior to the tank liner breaching because of contact with the reducing grout pore fluids. The grout pore fluids are in equilibrium with gibbsite and calcite throughout the simulation, so the presence of these in the residual waste layer do not affect the pore fluid composition. The effect of the other phases is unknown. Nonetheless, the residual waste layer is

approximately 2.9 cm thick on average (U-ESR-F-00041) compared to the approximate 10 meter thick layer of grout above it. Hence, 1 pore volume of fluid passing through the grout equates to approximately 345 pore volumes of the residual waste layer (assuming a similar porosity). So, the mineralogy of the residual waste layer should quickly approach equilibrium with the grout pore fluids.

Figures 3 and 4 show the evolution of Eh and pH in fluids eluting from the tank grout over 2500 pore volumes. Figure 5 shows the evolution of the mineralogy of the grout that dictates the pH and Eh transitions. In Denham (2007, Rev. 1), a nomenclature modified from Bradbury and Sarott (1995) was used to describe the chemical evolution of the tank grout and will be used here for consistency. The grout evolves through three distinct regions beginning with Reduced Region II (Figure 3). In this region the Eh is predominantly -0.47 volts and is poised by the presence of pyrite. When pyrite is completely oxidized at pore volume 523, there is a step change to Oxidized Region II with an Eh of +0.56 volts. Throughout Reduced Region II and Oxidized Region II, JenH and TobD control pH (Figure 5). Over most of these regions the pH is 11.1, controlled by TobD (Figures 4 and 5). At pore volume 2119 the mass of TobD is exhausted and the grout moves into Oxidized Region III. This region has an Eh of +0.68 volts and a pH of 9.2. The Eh is poised by equilibrium with dissolved oxygen and the pH is controlled by OH-hydrotalcite. An increase in total dissolved carbonate also occurs in Oxidized Region III as calcite begins to dissolve.

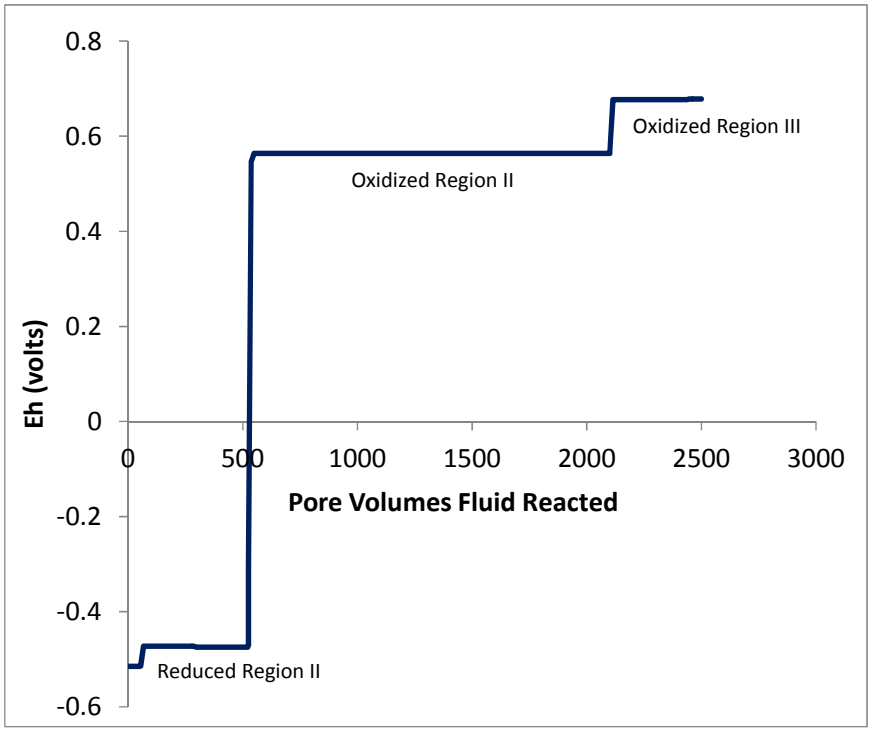

Figure 3: Simulated evolution of Eh in tank grout pore fluids entering residual waste layer.

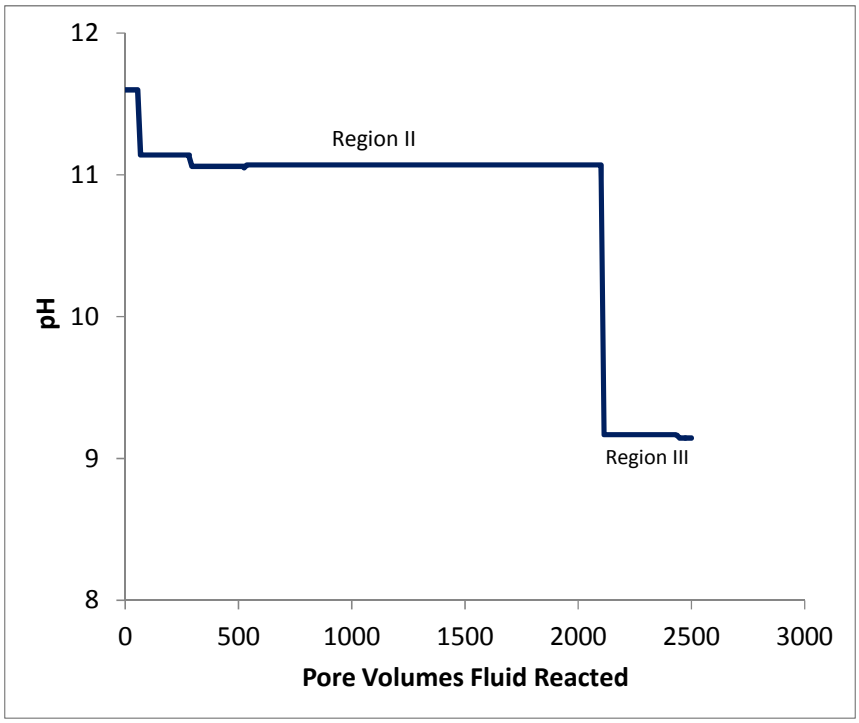

Figure 4: Simulated evolution of pH in grout pore fluids entering residual waste layer.

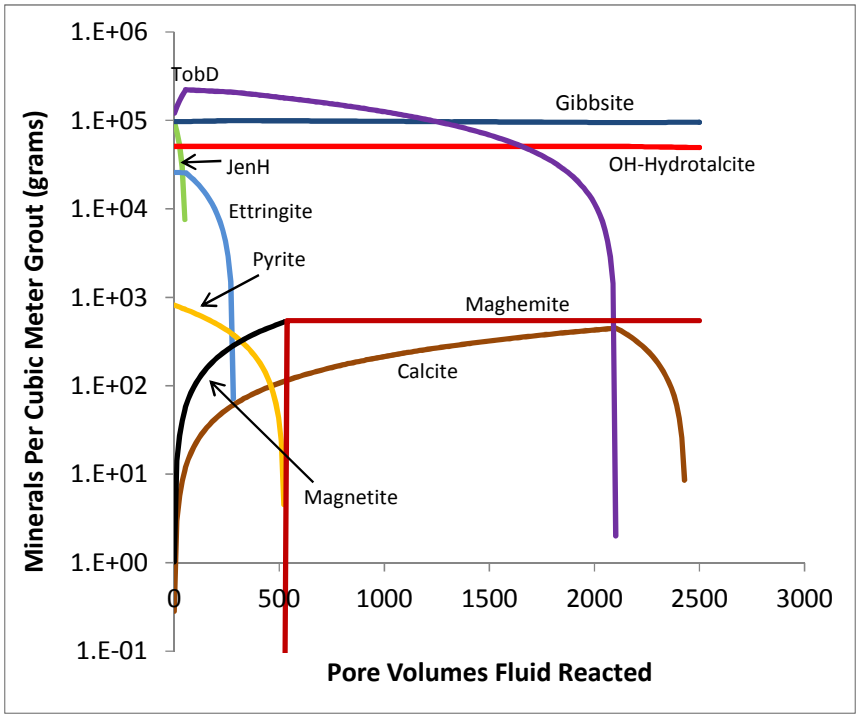

Figure 5: Simulated evolution of mineralogy in tank grout.

The simulation results provide the basis for choosing chemical conditions for calculating solubility of various radionuclides throughout the Performance Assessment modeling period. These are shown in Table 6.

Table 6: Eh, pH and total dissolved carbonate at different chemical conditions during simulated evolution of tank grout.

Chemical Condition	Eh (volts)	pH	Total Carbonate (molar)
Reduced Region II	-0.47	11.1	6.7E-7
Oxidized Region II	+0.56	11.1	6.9E-7
Oxidized Region III	+0.68	9.2	7.5E-5

Solubility of Plutonium

The waste release model for plutonium was updated using newer thermodynamic data than was used in Denham (2007, Rev. 1) and analyses of samples from FTF Tank 18. The thermodynamic data for plutonium is from the Nuclear Energy Agency (NEA) reviews of thermodynamic data (Lemire et al., 2001; Guillaumont et al., 2003) was recommended by a plutonium expert panel (Plutonium Solubility Peer Review Report, LA-UR-12-00079). The data was downloaded directly from the NEA website (http://www.oecd-nea.org/dbtdb/) in December of 2011. The "Pu Formation" database includes Gibbs free energies of aqueous and solid Pu species recognized by the NEA review. The recommended free energies for all hydroxide and carbonate aqueous complexes, as well as the solids $PuO_{2(am,hyd)}$ and $PuO_{2(cr),}$ were used to generate equilibrium constants for dissociation reactions for each species. These were then entered into the database created to run the grout simulations. In addition, the equilibrium constants for the species in the carbonate system were updated according to the NEA database. The additions to the database used for the simulations are shown in Appendix 2.

In Denham (2007, Rev. 1), solubilities of Pu in two forms were calculated – discrete phase $Pu(OH)_{4,}$ or in NEA parlance $PuO_{2(am,hyd)}$,and Pu coprecipitated with iron oxides. These forms are also used for the solubilities calculated here. The chemical conditions used for solubility calculations in Denham (2007, Rev. 1) were dictated by an earlier conceptual model in which pH was controlled by dissolution of portlandite in Region II and by calcite in Region III. These pH values were inconsistent with the grout modeling in which a form of C-S-H gel controlled the pH. Eh was controlled by pyrrhotite in the reducing stage and by equilibrium with dissolved oxygen in the oxidizing stage. For solubilities calculated here, pH values consistent with the grout modeling are used and Eh for reducing conditions is controlled by pyrite. For oxidizing conditions two sets of Eh values are used here. One is consistent with the grout simulations – equilibrium with dissolved oxygen – and one is considered more realistic.

Figure 6 shows the Pu solubilities for discrete $PuO_{2(hyd,am)}$ for chemical conditions throughout the grout simulations. As $PuO_{2(am,hyd)}$ ages it loses water, becomes more crystalline and is less soluble. The solubility of the crystalline form of PuO_2 is approximately 6 orders of magnitude

less than $PuO_{2(am,hyd)}$. Nevertheless, in the wet environment of a closed tank, the surface of any crystalline PuO_2 is likely to be hydrated (Hobbs, 2012). Thus, $PuO_{2(am,hyd)}$ is the appropriate solid to use in solubility calculations to control solubility of discrete phase plutonium.

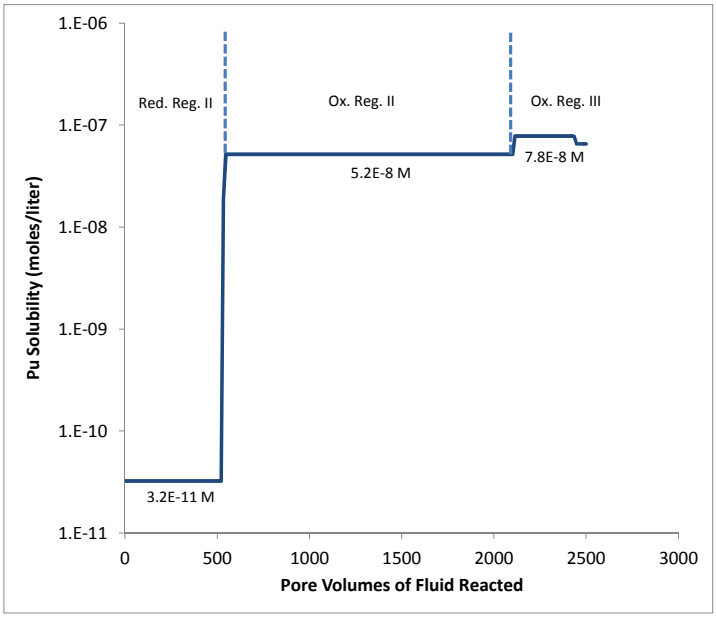

Figure 6: Calculated solubility of discrete phase $PuO_{2(am,hyd)}$ during chemical evolution of pore fluids.

Plutonium solubility is very sensitive to Eh at highly oxidizing conditions. Figure 7 shows the solubility of $PuO_{2(am,hyd)}$ versus Eh at a pH and total carbonate concentrations commensurate with those of Oxidized Region II and III. Slight changes in Eh above a value of 0.45 volts result in large changes in $PuO_{2(am,hyd)}$ solubility. The Eh that results from the grout simulations is in equilibrium with dissolved oxygen, and hence the maximum Eh possible in an aqueous system. This results in solubilities in the oxidized regions that are maximums.

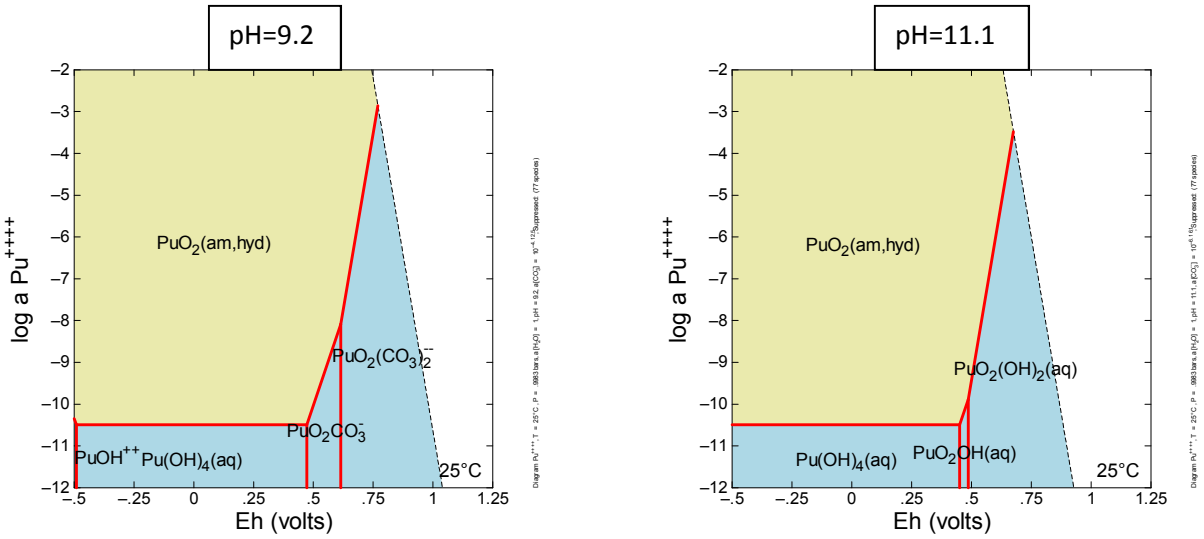

Figure 7: Log [Pu] v. Eh at pH=9.2, [CO3tot]=7.5E-5 moles/liter (left) and pH=11.1, [CO3tot]=6.9E-7 moles/liter (right). Note that log a Pu++++ represents total Pu.

The Eh values of natural waters are rarely in equilibrium with dissolved oxygen, predominantly because of slow reaction kinetics for oxidation by dissolved oxygen (Langmuir, 1997). Figure 8, from Langmuir (1997), shows Eh-pH regimes for different types of natural waters. The added red ovals are at pH values of approximately 9.2 and 11.1 and suggest the range of Eh values that would be reasonable for calculating solubilities at these pH values. The disparity between measured Eh and that in equilibrium with dissolved oxygen is also observed in SRS groundwater. Eh measurements of groundwater from 6 water table wells reported in Stom and Kaback (1992) are shown on an Eh-pH diagram in Figure 9. The Eh values are lower than would be expected for equilibrium with dissolved oxygen (cross-hatched region) and their position suggests they reflect the ferric-ferrous iron couple. Others have suggested that Eh values used for modeling metal solubility and speciation in cements at pH=12.5 should be near +0.2 volts (Glasser, 1997; Krupka and Serne, 1998), rather than the +0.48 volts that would be in equilibrium with dissolved oxygen. Atkins and Glasser (1992) reported that Eh values of ordinary Portland cement should be between 0 and +0.1 volts. Therefore, it is reasonable to assume that Eh values controlling solubility in the oxidized regions simulated here would be lower than those resulting from the grout simulations (i.e., lower than equilibrium with the dissolved oxygen).

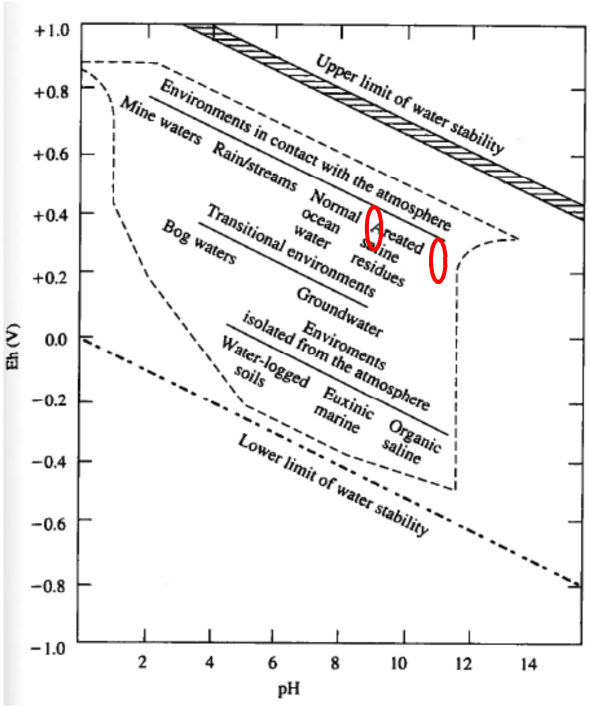

Figure 8: Eh-pH diagram from Langmuir (1997) showing typical regimes for various natural waters; red ovals are overlaid to suggest range of realistic Eh values for calculating solubilities in Oxidized Region II and III.

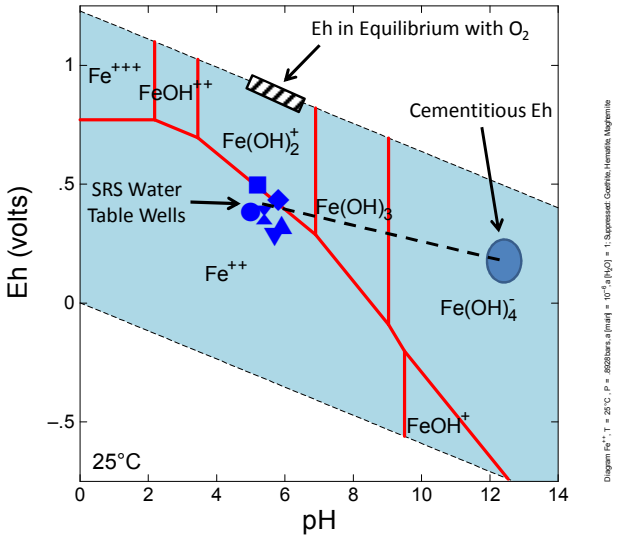

Figure 9: Eh-pH diagram showing Eh of SRS background water table wells in relation to iron speciation.

The values of Eh chosen to calculate $PuO_{2(am,hyd)}$ solubility in Oxidized Regions II and III are not critical as long as they are below +0.45 volts (Figure 7). Here, Eh values of +0.24 and +0.29 volts were chosen for Oxidized Regions II and III. This was based on extrapolating the groundwater values from Figure 9 to the appropriate pH values of 11.1 and 9.2 along a line intersecting the point pH=12.5, Eh=+0.2 v. At these lower Eh values the solubility of $PuO_{2(am,hyd)}$ is a constant 3.2E-11 moles/liter across the three chemical regimes – Reduced Region II, Oxidized Region II, and Oxidized Region III.

The term coprecipitated used in Denham (2007, Rev. 1) was inclusive of plutonium bound in the crystal lattice of solid iron phases and mixed with iron phases such that the access of pore fluids to the plutonium is occluded by the host phase. There is indirect evidence to suggest that plutonium would be coprecipitated with iron phases. Coprecipitation with ferric iron phases has been the basis for various methods of removal of plutonium from solution (e.g., Gävfert et al., 2002; Slater et al., 1997; Lozano et al., 1997). Site specific evidence is presented in a review of Tank 18 history and chemistry by Hobbs (2012). He concludes that it is likely that a portion of plutonium remaining in the residual waste after cleaning is coprecipitated.

The concentration at which coprecipitated plutonium would be released from a host iron phase – the apparent solubility -- is unknown. Nevertheless, if it is assumed that plutonium would be released as the iron phase dissolved at the same molar Pu:Fe ratio at which it exists in the solid, an apparent solubility can be estimated. The average Pu:Fe ratio in 6 samples from the residual waste layer in Tank 18 is 4.1E-4 (Oji et al, 2010). Hence, an estimation of the solubility of the iron phase at the different conditions multiplied by the Pu:Fe ratio in the waste would estimate the apparent solubilities of plutonium coprecipitated with iron at the different chemical

conditions. A similar method was used by Cantrell et al. (2006) to calculate release of Tc-99 from an iron phase.

The iron phases used here to estimate the apparent solubility of coprecipitated plutonium throughout the post-closure aging of the tanks are magnetite (Fe_3O_4) and maghemite (Fe_2O_3). X-ray diffraction analysis of Tank 18 residual waste samples by Hay (2012) show that hematite is a dominant iron phase in the tank today. For the grout simulations presented here it is assumed that exposure to reducing pore fluids after closure, but before the liner is breached, would convert the hematite to magnetite. Magnetite is assumed to be prevalent in Reducing Region II and oxidizes to maghemite at the transition to Oxidized Region II. Denham (2007, Rev. 1) assumed prevalence of hematite in Oxidized Region II and III, but maghemite is a more likely oxidation product of magnetite because of their similar crystal structures. In addition, maghemite is more soluble than hematite and biases the apparent solubilities of plutonium to higher values.

The solubilities of magnetite and maghemite were calculated at the chemical conditions of Reduced Region II, Oxidized Region II, and Oxidized Region III using The Geochemist's Workbench®. Thermodynamic data for magnetite was obtained from the HATCHES database (Heath, 2007). For comparison, the solubility of magnetite using a value for logK from the HSC v.7 database (Roine, 2009) was slightly higher (6.8E-6 versus 4.0E-6) than that from Geochemist's Workbench®. The value from the HATCHES database was used because it is expected to be more consistent with the NEA thermodynamic data. Neither the HATCHES nor the NEA databases contain data for maghemite. Thus, the thermodynamic data for this phase was obtained from the HSC v. 7 database. Table 7 shows the solubility of the iron host phase and the apparent solubility of plutonium at the three regions of grout aging.

Table 7: Solubilities of iron host phase and apparent solubilities of coprecipitated plutonium throughout tank grout aging.

Grout Aging Region	Magnetite Solubility (moles/liter)	Maghemite Solubility (moles/liter)	Pu Apparent Solubility (moles/liter)
Reduced II	7.2E-11	----	3.0E-14
Oxidized II	----	6.1E-10	2.5E-13
Oxidized III	----	1.2E-11	5.0E-15

The estimation of waste release concentrations of plutonium during aging of Tank 18 presented here assumes that plutonium is present as either the discrete phase $PuO_{2(am,hyd)}$ or coprecipitated with iron phases. In reality, plutonium is likely to exist in both these forms and perhaps others discussed in the uncertainty section. As long as pore waters are contacting a sufficient surface area of $PuO_{2(am,hyd)}$, the release concentration will be dominated by the solubility of $PuO_{2(am,hyd)}$. If the surface area of discrete particles available to pore fluids decreases to a point that saturation with $PuO_{2(am,hyd)}$ cannot be maintained, the release concentration of plutonium would be controlled by the coprecipitated form (i.e., controlled through occlusion by the host iron phase). Without experimental evidence to inform, the summary waste release concentrations presented in

Table 8 can be viewed as two end-members with an intermediate case. The solubility of discrete $PuO_{2(am,hyd)}$ at equilibrium with dissolved oxygen is the maximum waste release concentration and coprecipitation is the minimum. For the oxidized regions, the solubility of $PuO_{2(am,hyd)}$ at Eh values of +0.24 and +0.29 volts represents a more realistic minimum.

Table 8: Summary of estimated waste release concentrations of plutonium during Tank 18 aging.

Grout Aging Region	$PuO_{2(am,hyd)}$ Max[a] (moles/liter)	$PuO_{2(am,hyd)}$ More Realistic[b] (moles/liter)	Coprecipitated (moles/liter)
Reduced Region II	3.2E-11	3.2E-11	3.0E-14
Oxidized Region II	5.2E-8	3.2E-11	2.5E-13
Oxidized Region III	7.8E-8	3.2E-11	5.0E-15

a—Eh values in equilibrium with dissolved oxygen

b—more realistic Eh values (explained in text)

Uncertainties

Simulation of Chemical Evolution of Tank Grout

This simulation of the chemical evolution of tank grout is meant to provide a basis for Performance Assessment modeling to change solubility of radionuclides in the residual waste layer in response to changes in fluid composition passing through this layer. There is considerable uncertainty in this approach that cannot be quantified. This is primarily driven by the lack of knowledge of the physical condition of the grout at the time the liner is breached and thereafter. To date Performance Assessment modeling of the F-Area tanks has treated the grout as a porous medium and the effect of fast flow paths and other phenomena have been assessed in sensitivity analyses. The simulation of the chemical evolution of tank grout presented here is consistent with treatment of the grout as a porous medium and does not account for physical degradation of grout or heterogeneity in chemical or flow properties.

For comparison, other studies have considered migration rates of an oxidation front and a pH front caused by diffusion of oxygen and carbon dioxide into tank grout from the vadose zone. Kaplan et al. (2005) considered diffusion of oxygen from the vadose zone and the resulting migration of an oxidation front. Langton (2007) considered the advancement of a pH front caused by acid attack and carbonation (at 50% water saturation). In both cases, the advance of the degradation front was very slow. Though their results are not directly comparable to the simulations presented here, Kaplan et al. (2005) and Langton (2007) provide context on how different processes, not considered here, would affect the chemical evolution of the grout.

There are also uncertainties associated with the simulations presented here that are summarized below.

The Eh transition is primarily controlled by the amount of slag used in the grout formulation, its reduction capacity, the amount of that reduction capacity imparted to the grout, and the

thermodynamic data used for pyrite. It has been assumed here that all reduction capacity measured in the slag would be imparted to the grout. It is possible that not all of this reduction capacity would be available to pore waters and the Eh transition would occur at fewer pore volumes of infiltrating fluid. However, it is interesting to note that Roberts and Kaplan (2009) found that the reduction of Saltstone and Saltstone vault concrete exceed that expected based on the amount of slag in these cementitious forms. It could be argued that for Saltstone, the simulant fluids used in the formulation had high concentrations of nitrite that could act as a reductant. However, the nitrite concentrations in the different simulants varied by a factor of 4, with no corresponding variation in reduction capacity of the Saltstone. Furthermore, nitrite does not explain the elevated reduction capacity of the vault concrete. Nevertheless, in the current simulations, this possibility is compensated for by accounting for just the reduction capacity imparted by the blast furnace slag. Both the Portland cement and fly ash have substantial reduction capacity as well (Roberts and Kaplan, 2009). Fly ash has only 36% of the reduction capacity of blast furnace slag, but makes up a higher fraction of the cementitious materials in the tank grout. Figure 6 shows the results of the simulation using slag alone and adding in the reduction capacity of the fly ash using the mineral magnetite. In this simulation, the Eh mimics the original simulation (Figure 3) until 523 pore volumes of fluid have reacted. Then, the Eh rises to -0.26 volts and is maintained for an additional 352 pore volumes. At 875 pore volumes, the Eh rises to +0.56 volts.

The equilibrium constant for the reaction:

$FeS_2 + 2H^+ + 2e^- = Fe^{+2} + 2HS^-$

varies by 2 orders of magnitude depending on the thermodynamic database used. In Denham (2007, Rev. 1) the thermodynamic database “thermo.com.V8.R6+” was used with logK= -16.23 for the pyrite dissolution reaction. Newer thermodynamic databases use lower logK values for pyrite dissolution. Hummel (2002) used logK= -18.50, while the HATCHES database uses a value of logK= -17.49. The value from the HATCHES database was chosen here because it is in between the two extremes. It also agrees with the value reported for this reaction by the HSC v.7.0 thermodynamic database. This accounts for some of the difference between the value of the Eh change in the current simulations compared to those in Denham (2007, Rev.1). In that previous document the transition occurred at 371 pore volumes rather than 523. The remainder of the difference is the result of underestimating the amount of pyrrhotite required to account for the reducing capacity of the slag in Denham (2007, Rev. 1). The grout formulation used in that report does not differ significantly in the fraction of slag from that used in the current simulations.

Another factor that significantly affects the redox transition is the dissolved oxygen concentration in the assumed infiltrating water. The concentration used was in equilibrium with atmospheric oxygen – the highest possible concentration. The number of pore volumes required to reach the redox transition is inversely proportional to the dissolved oxygen concentration in

the infiltrating water. Hence, at lower dissolved oxygen concentrations the number of pore volumes of infiltrating fluid required to cause the redox transition would be proportionally higher. A survey of dissolved oxygen concentrations in SRS background wells screened in the water table aquifer showed that they are close to saturation with atmospheric oxygen (Millings, 2011). Nevertheless, there were wells that had concentrations that were nearly 40% less than saturation. Thus, the value of dissolved oxygen concentration assumed for infiltrating water is reasonable, but it should be noted that it could be lower.

The pH transition (Region II to Region III) is controlled primarily by the amount of hydrous calcium silicates present in the grout, but other factors have secondary effects. The total dissolved carbonate concentration exerts some control on the pH transition, though it is relatively minor. Increasing the dissolved carbonate concentration by an order of magnitude reduces the number of pore volumes required to achieve the pH transition by only 5%. An increase of 2 orders of magnitude results in a 30% decrease in the number of pore volumes required to reach the transition. This is because carbonation is not the major reaction controlling dissolution of the hydrous calcium silicates. If it were, calcite would precipitate at near stoichiometry with dissolution of TobD, but Figure 5 indicates that the amount of calcite precipitating is much less that the amount of TobD dissolved.

The concentration of dissolved silica in the infiltrating water has a more significant influence on the pH transition by suppressing the dissolution of hydrous calcium silicates. The infiltrating water was assumed to be in equilibrium with amorphous silica, which produces the highest reasonable dissolved silica concentration. Were it in equilibrium with a lower solubility form of silica such as cristobalite, the number of pore volumes of infiltrating fluid required to reach the pH transition would be 16% higher. The transition would occur at a still higher number of pore volumes if the infiltrating water were assumed to be in equilibrium with quartz.

A more influential control on the pH transition is the disposition of silica in the simulation. The base case simulation was done assuming the silica in the grout was essentially inert and was thus not an input into the original mineralogy. Only one phase can be input as the “basis” for each chemical component. To allow for the input of a calcium sulfate phase (gypum) and a hydrous calcium silicate phase, the silica in the grout composition was left out of the simulation. This has various effects depending on the assumed form of the silica. Figure 10 shows the effects of different scenarios involving silica compared to the base case in which silica was not included in the initial mineralogy. When silica is added it complicates the pH transition because three distinct pH regions occur, the duration and pH values varying with the form of silica. If silica from the normative mineralogy calculation is added as amorphous silica, the first pH transition from 11.0 to 9.8 occurs at approximately 50% fewer pore volumes of fluid reacted. The second transition from a pH value of 9.8 to 9.1 occurs at 4198 pore volumes. However, if kaolinite is allowed to precipitate the first transition occurs at transition at only 13% fewer pore volumes. If the form of silica is the more stable cristobalite, there is a minor pH transition from 11.0 to 10.7 at 1109 pore volumes, but the major transition from 10.7 to 9.3 occurs at 2389 pore volumes. If

quartz is assumed to account for the silica, the transitions are very near those of cristobalite. Given the time frame of hundreds to thousands of years, silica in the original grout may recrystallize as cristobalite or quartz. In any event, the case chosen – to eliminate a silica phase from the original mineralogy – is the simplest and represents a middle ground.

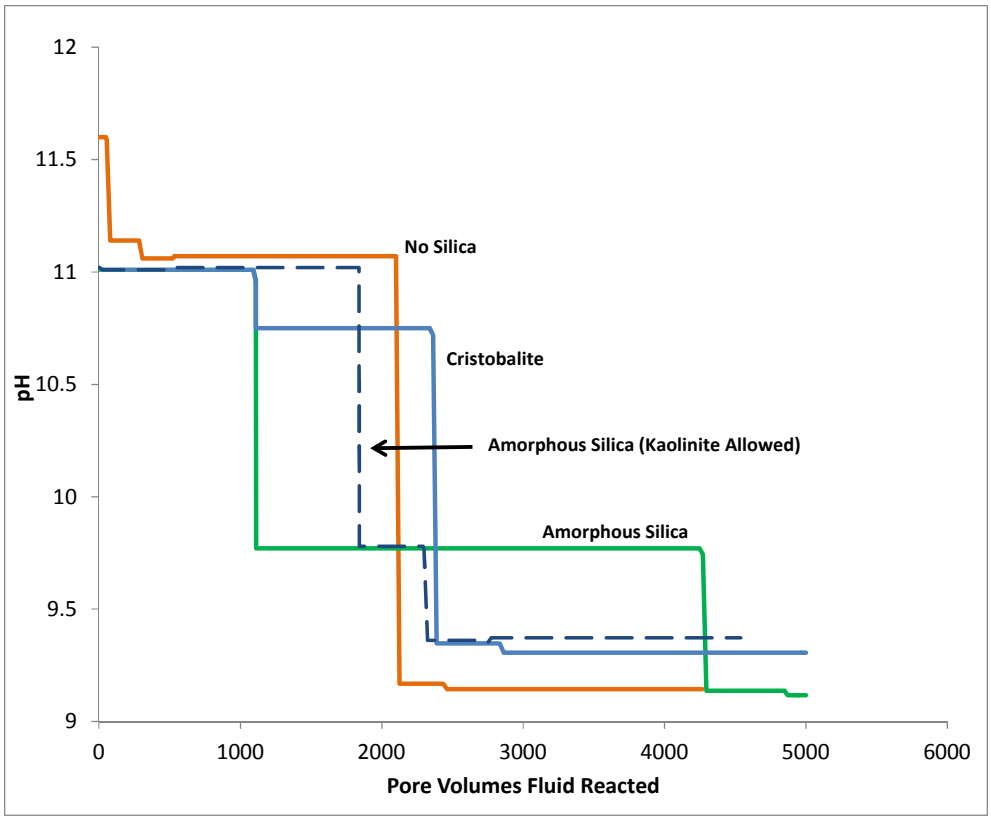

Figure 10: Results of different scenarios for inclusion of the normative silica in the grout evolution simulation.

Uncertainties in Plutonium Solubility Estimates

There are several sources of uncertainty in the estimates of plutonium solubility presented here. Some stem from uncertainty in the modeling of grout aging, but the primary source is the solid form the plutonium will be in when the tank liner fails. The following points discuss these uncertainty issues.

Solid Plutonium Form

$PuO_{2(am,hyd)}$ was assumed to be the form plutonium will take if it is in discrete particles. It is the most soluble of the reasonable forms for the relevant conditions. $PuO_{2(am,hyd)}$) is known to dehydrate and become less soluble as it ages. The final product of the aging is crystalline PuO_2 that up to six orders of magnitude less soluble than $PuO_{2(am,hyd)}$. However, as Hobbs (2012) discussed, in a wet environment the completely dehydrated and crystalline form will never be

reached. Nonetheless, it is unknown whether some dehydration may occur shortly after grout is poured due to elevated temperatures and pressures or whether partial crystallization would occur with tank aging (Hobbs, 2012). If these processes occur, they would tend to lower the solubility of plutonium.

Plutonium coprecipitated in iron minerals is the other form considered here. By the definition used here, coprecipitation means plutonium bound in an iron phase that is occluded from reacting with pore fluids. It only reacts as the iron host phase is dissolved. The mechanism is not specified. Plutonium could be bound in the crystal lattice of the iron phase, it could be adsorbed to iron phase particles that are agglomerated together to form the residual waste layer, or it could occur as small discrete plutonium particles surrounded by the host iron phase. Recent characterization of Tank 18 residual waste samples by Hay (2012) show plutonium in discrete <1 μm particles embedded in much large particles dominated by iron. This was the only plutonium observed in SEM analysis with elemental analysis capability. It is unclear whether dissolution of these particles would depend on dissolution of the host or whether they would behave as discrete particles. It also doesn't preclude the occurrence of plutonium in the other forms considered here as coprecipitated.

The assumption used here to estimate an apparent solubility of coprecipitated plutonium is that plutonium is released into the pore fluid, as the iron phase dissolves, in the same Pu:Fe molar ratio as exists in the host solid. This assumption is the most valid for plutonium bound in the crystal lattice of the iron phase with a distribution coefficient of 1. Depending on plutonium concentration, distribution, and fluid flow through the residual layer, it could approximate the apparent solubility for other mechanisms as well. This said, the estimate of apparent solubility presented here probably represents the lower bounding value for apparent solubility of coprecipitated plutonium. The upper bounding value is the solubility of $PuO_{2(am,hyd)}$.

No adsorption of plutonium onto the residual waste layer is considered. In this waste release model when plutonium is dissolved from the host phase, it is released from the tank unimpeded. In reality, it would be subject to retardation caused by adsorption to the minerals of the residual waste layer.

Recent characterization data of Tank 18 residual waste samples suggests that another form of plutonium may occur in the tanks today. Hobbs (2012) hypothesizes that any discrete particles of plutonium in the tank today may be a carbonate form such as $Pu(OH)_2CO_3$ or $PuOCO_3$. This is based on the carbonate concentration in water separated from Tank 18 residual waste samples (Oji et al., 2009) and the identification of a uranyl carbonate phase, $Na_4UO_2(CO_3)_2$, by X-ray diffraction powder pattern. Formation of a plutonium carbonate species is consistent with behavior predicted by plutonium thermodynamics. The analyses of liquid reported in Oji et al. (2009) were charge balanced on OH- to obtain a pH of 10.2. This was used to construct the diagrams in Figure 11 using The Geochemist's Workbench®. These diagrams show that $Pu(OH)_2CO_3$ is the stable phase at the dissolved carbonate concentrations of the two liquid

samples (0.04 moles/liter). However, two factors suggest that $PuO_{2(am,hyd)}$ will be the stable phase at conditions in the tank after closure. The dissolved carbonate concentration in the residual waste layer will decrease because any dissolved or soluble carbonate will react with grout influenced pore fluids or with the grout itself to form calcium carbonate. Carbonate concentrations in equilibrium with calcium carbonate in the pH range of 10 to 11 are $<10^{-3}$ moles/liter and Figure 11 indicates that, below this concentration, $PuO_{2(am,hyd)}$ will be the stable phase. Likewise, pH will increase to 11.1 because of the influence of the grout. Figure 12 suggests that even at relatively high dissolved carbonate concentrations the stable phase will be $PuO_{2(am,hyd)}$ after tank closure.

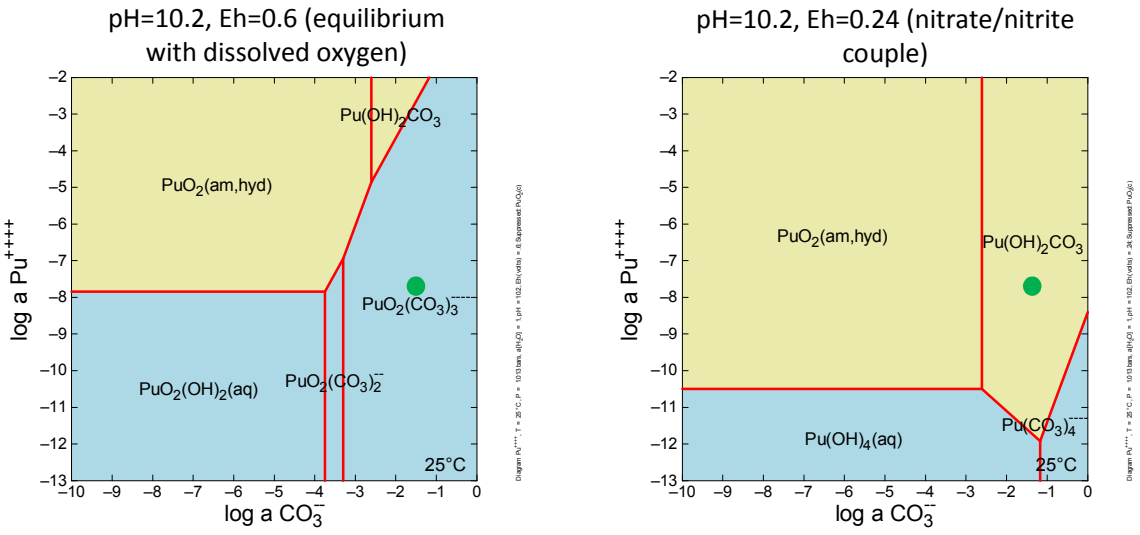

Figure 11: Pu versus log aCO_3^{-2} at a pH=10.2 and two different Eh values; green dot show the composition of the fluids in Oji et al. (2009). Note that Pu++++ represents total dissolved plutonium.

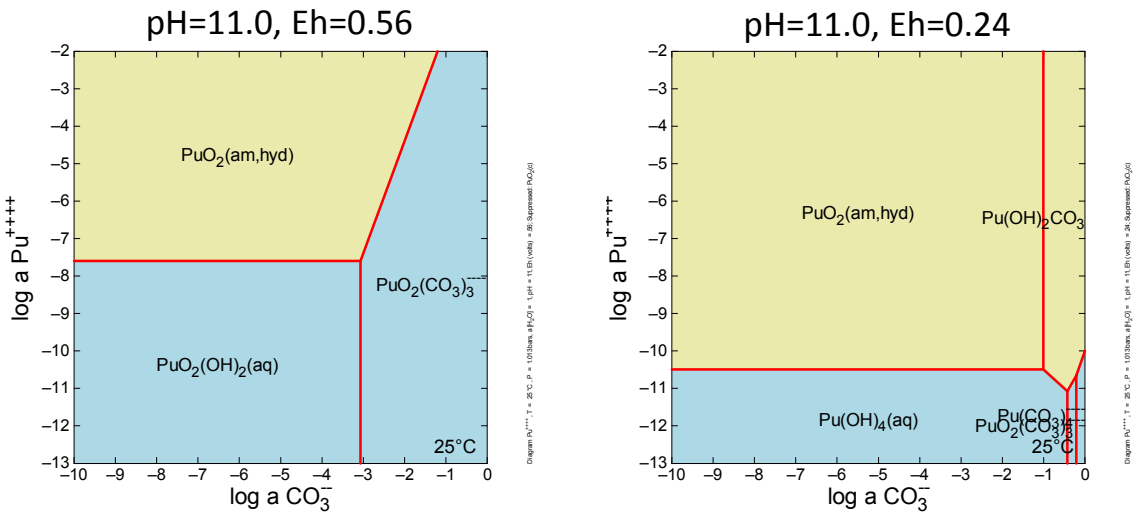

Figure 12: Pu versus log aCO_3^{-2} at pH 11 and Eh values in equilibrium with dissolved oxygen and the more realistic +0.24v. Note that Pu++++ represents total dissolved plutonium.

Effect of pH Variation

Mineralogy of the grout can affect the pH of the pore fluids. The assumption applied here is that after sitting in the tank for decades to thousands of years before breaching of the liner, the grout will be fully hydrated. The initial pH in the simulations is approximately 11.7, but while still in Reduced Region II, it decreases to 11.1. The pH stays at 11.1 throughout Oxidized Region II and decreases to 9.2 in Oxidized Region III. However, it is worth examining the effect of small variations in pH on $PuO_{2(am,hyd)}$ solubility.

Figure 13 displays the plutonium concentration in equilibrium with $PuO_{2(am,hyd)}$ versus pH at an Eh of -0.47 volts and a total carbonate concentration of 6.7E-7 moles/liter (Reduced Region II conditions). The pH can vary significantly in either direction from 11.1 without the solubility of $PuO_{2(am,hyd)}$ changing.

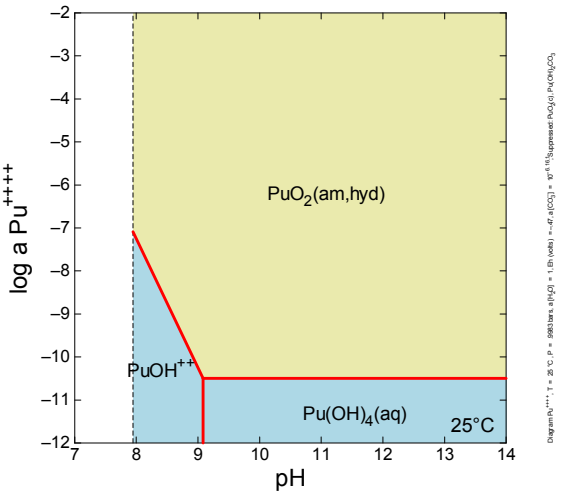

Figure 13: Log aPu versus pH with other parameters equivalent to those of Reduced Region II; note Pu++++ represents total plutonium.

For Oxidized Region II, plutonium solubility was calculated at an Eh in equilibrium with dissolved oxygen and a more reasonable Eh of 0.24 volts. Figure 14 shows the effects of pH variations at these conditions. At an Eh in equilibrium with dissolved oxygen (Eh=+0.56 volts), a pH of 11.1 (Oxidized Region II) lies on the sloped line defining the solubility of $PuO_{2(am,hyd)}$. If pH is greater than 11.1 the solubility will be higher. If it is less than 11.1 the solubility will be lower. At an Eh of +0.24 volts pH variation does not change the plutonium solubility.

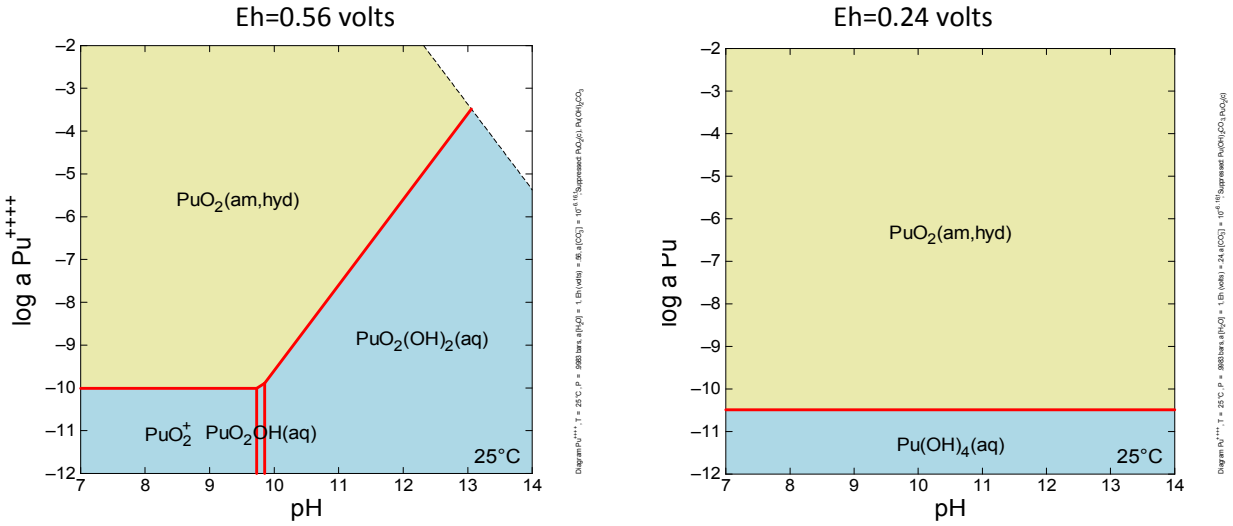

Figure 14: Log aPu versus pH for two Eh values and a total carbonate concentration of 6.9E-7 moles/liter; note that Pu++++ represents total plutonium.

In Oxidized Region III (see Figure 15), the effect of pH variation is similar to that in Oxidized Region II. From the Oxidized Region III pH of 9.2 and an Eh of +0.68 (equilibrium with dissolved oxygen), an increase in pH increases the solubility of $PuO_{2(am,hyd)}$; a decrease in pH decreases the solubility. At an Eh of +0.4 volts wide variations of pH around 9.2 can occur without changing the solubility of $PuO_{2(am,hyd)}$.

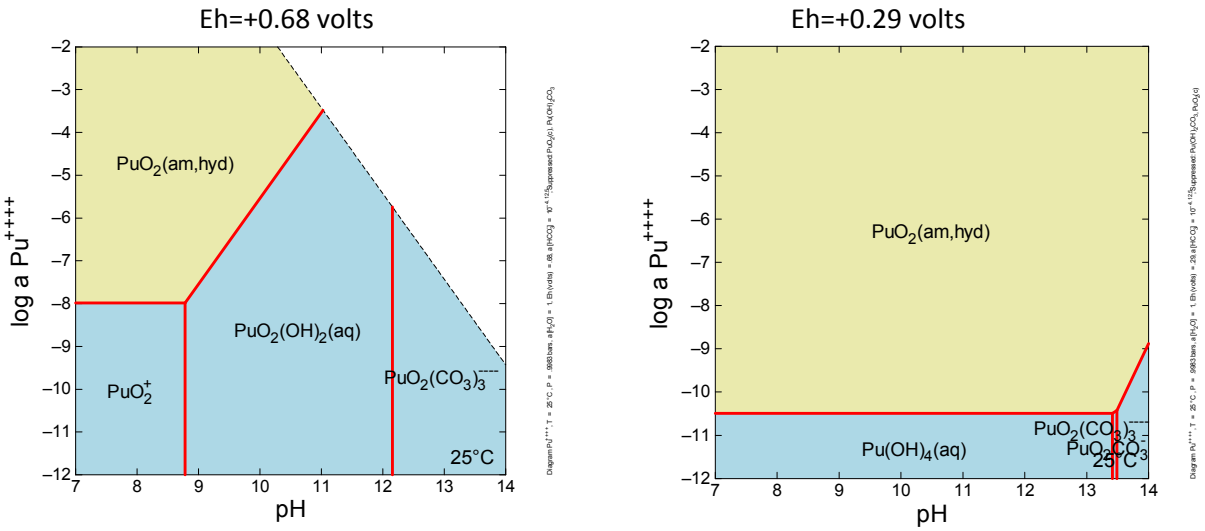

Figure 15: Log aPu versus pH for two Eh values and a total carbonate concentration of 7.5E-5 moles/liter; note that Pu++++ represents total plutonium.

Effect of the Treatment of Silica in Grout Modeling

As discussed in the section on uncertainty in grout modeling, the way silica is treated in the mineralogy has an effect on the pH transition. However, it has minimal effect on the solubility of $PuO_{2(am,hyd)}$ (Figure 16). The transition to the plutonium solubility for Oxidized Region III actually occurs after many more pore volumes of infiltrating fluid have reacted when amorphous silica is used in the initial mineralogy.

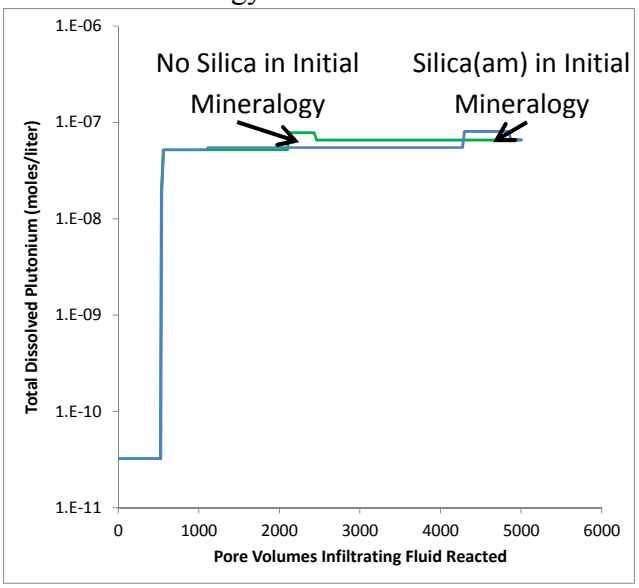

Figure 16: Effect of the treatment of silica in the initial mineralogy of the grout aging simulations.

Uncertainty in Thermodynamic Data

The NEA database includes estimated uncertainties in the free energies of each aqueous and solid plutonium species. These were used to calculate uncertainties in the overall solubility of $PuO_{2(am,hyd)}$ at the conditions of interest. This was done by calculating the uncertainty in the LogK for the dissociation reactions of the four dominant aqueous species and $PuO_{2(am,hyd)}$. The LogK values for these reactions were used in The Geochemist's Workbench® and solubilities were calculated to provide the maximum change in solubility in both directions. For Eh values considered more reasonable, the uncertainty around the solubility of 3.2E-11 is +7.8E-11 and -2.2E-11. For Eh values in equilibrium with dissolved oxygen the uncertainty in the solubilities calculated in the oxidized regions are much higher -- up to 2 orders of magnitude. This is because the uncertainty in the LogK of the dissociation reaction of the aqueous species $PuO_2(OH)_{2(aq)}$ dominates and is approximately 2 orders of magnitude in each direction.

Effect of High Carbonate Concentrations

At pH 11.1 and Eh in equilibrium with dissolved oxygen, the solubility of $PuO_{2(am,hyd)}$ increases as dissolved carbonate concentration increases because of carbonate complexing of Pu(VI). However, reactions will occurthat will tend to mitigate the effects of elevated carbonate concentrations. As long as the hydrous calcium silicate TobD is present it will react with carbonate to form calcite, buffering the dissolved carbonate to low values. If ToD is unavailable, rising carbonate concentrations cause the pH to decrease, increasing the stability of $Pu(OH)_2CO_{3(s)}$. For example, in Oxidizing Region III, increasing total dissolved carbonate to approximately $10^{-3.7}$ moles/liter would cause the hydroxy carbonate to become stable (Figure 17). At an Eh in equilibrium with dissolved oxygen, this would reduce the effect on plutonium solubility. At a more realistic Eh of +0.29 volts, high total dissolved carbonate further stabilizes the plutonium hydroxy carbonate and actually reduces the solubility of plutonium.

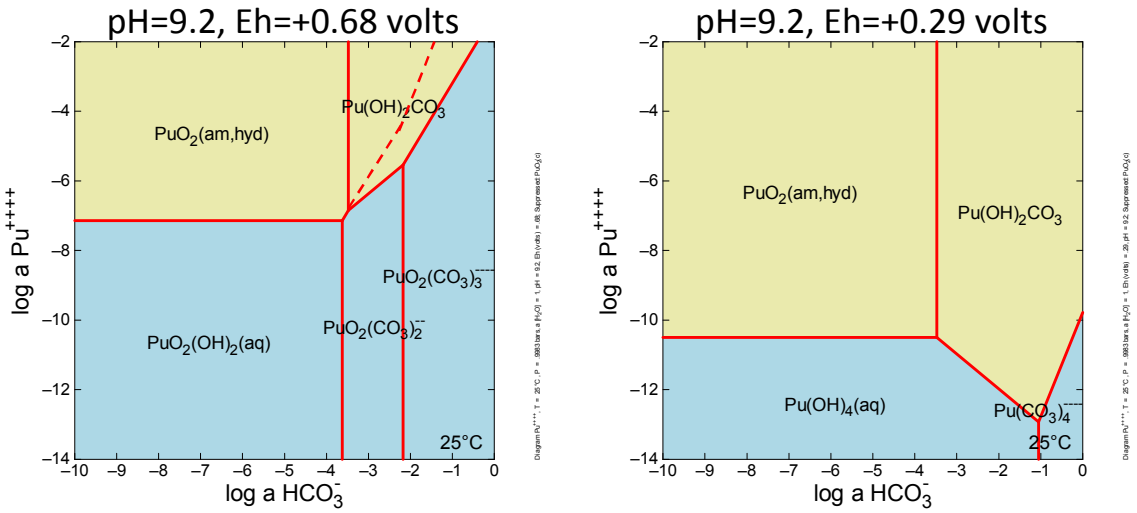

Figure 17: Log aPu versus log $aHCO_3^-$ at pH=9.2 and two Eh values; dashed line at Eh=+0.68 volts shows solubility of $PuO_{2(am,hyd)}$ in the absence of $Pu(OH)_2CO_3$.

Conclusions

The information presented here is intended to provide bounding values of plutonium solubility for use in assessing the post-closure performance of Tank 18 and 19 of the F-Tank Farm. The grout simulations provide an estimate of major pore fluid changes throughout the assessment period which, in turn, allow for bounding plutonium solubilities to vary as the tank grout ages. The information can be used in a flow and transport model that converts into time the number of pore volumes of infiltrating fluid required to reach each major transition in pore fluid composition. The model can then apply the corresponding plutonium solubility resulting in varying plutonium flux from the tank as it ages.

Simulations of the effects of grout aging on pore fluids controlling the solubility of plutonium and the resulting plutonium solubilities were calculated based on new information. For the grout simulations, newer and more widely accepted thermodynamic data for cementitious minerals were used, as was a new grout formulation for Tanks 18 and 19. Likewise, newer and more widely accepted thermodynamic data for plutonium were used to calculate solubilities for the discrete plutonium phase $PuO_{2(am,hyd)}$. Pu:Fe ratios from analyses of Tank 18 residual waste samples were used to estimate apparent solubilities of coprecipitated plutonium. The results are shown below:

Grout Aging Region	Transition in Pore Volumes	$PuO_{2(am,hyd)}$ Max[a] (moles/liter)	$PuO_{2(am,hyd)}$ More Realistic[b] (moles/liter)	Coprecipitated (moles/liter)
Reduced Region II	1 to 523	3.2E-11	3.2E-11	3.0E-14
Oxidized Region II	524 to 2119	5.2E-8	3.2E-11	2.5E-13
Oxidized Region III	>2119	7.8E-8	3.2E-11	5.0E-15

The solubility of $PuO_{2(am,hyd)}$ was estimated at two different Eh values. The first was an Eh value in equilibrium with dissolved oxygen. These values are considered maximums because the Eh value is unlikely to be that high because oxidation by dissolved oxygen tends to be slow. More realistic Eh values were estimated based on studies of cementitious systems. At the more realistic Eh values the solubilities in the oxidized regions are approximately 3 orders of magnitude lower and are equal to that estimated for Reduced Region II. The thermodynamics of plutonium suggest that below an Eh of approximately +0.45 volts the solubility is not sensitive to Eh. It was also shown that at these more realistic Eh values, the solubility is not sensitive to variations in pH or variations in total dissolved carbonate concentration.

The primary uncertainty associated with both the grout simulations and the plutonium solubility estimations is the nature of the grout and the plutonium in the future. Little is known about the degree of fracturing or the character of fractures that will occur in the grout in the distant future. The simulations treat the grout as a porous medium and there is no consideration of the physical degradation. It is known that some of the plutonium in the residual waste today occurs as micrometer sized discrete particles embedded in a matrix rich in iron. The exact plutonium phase is unknown, but the argument is made here that after closure the plutonium form is likely to be discrete particles of $PuO_{2(am,hyd)}$, plutonium coprecipitated with iron, or both. It is possible that some dehydration and/or crystallization of the $PuO_{2(am,hyd)}$ will occur with time, resulting in lower solubilities for discrete plutonium particles. Yet, these solubilities are not likely to ever decrease to that of crystalline PuO_2.

References

Atkins, M. and F.P. Glasser, 1992. Application of Portland cement-based materials to radioactive waste immobilization. *Waste Management*, 12, 105-131.

Bethke, C.M.and S. Yeakel, 2009. The Geochemist's Workbench® (geochemical modeling software), Release 8.0 Reference Manual, University of Illinois.

Bradbury, M. H., Sarott, F., 1995. Sorption Database for the Cementitious Near-Field of a L/ILW Repository for Performance Assessment, PIT-MISC-0075, ISSN 1019-0643, Paul Scherrer Institut, Switzerland.

Cantrell, K.J., K.M. Krupka, W.J. Deutsch, and M.J. Lindberg, 2006. Residual waste from Hanford tanks 241-C-203 and 241-C-204. 2. Contaminant Release Model, *Environmental Science and Technology*, 40, 3755-3761.

Gäfvert, T., C. Ellmark, and E. Holm, 2002. Removal of radionuclides at a waterworks. *Journal of Environmental Radioactivity*, 63, 105-115.

Denham, M., 2007. Conceptual Model of Waste Release from the Contaminated Zone of Closed Radioactive Waste Tanks. WSRC-STI-2007-00544, Rev. 1, Washington Savannah River Company, Aiken, SC.

Glasser, F.P., 1997. Fundamental aspects of cement solidification and stabilization. *Journal of Hazardous Materials*, 52, 151-170.

Guillaumont, R., T. Fanghänel, J. Fuger, I. Grenthe, V. Neck, D.A. Palmer, M.H. Rand, 2003. Update on the Chemical Thermodynamics of Uranium, Neptunium, Plutonium, Americium, and Technetium, Chemical Thermodynamics 5. Elsevier.

Heath, T., 2007. The HATCHES User Manual. Serco Assurance, Oxfordshire, England.

Hay, M.S., P.E. O'Rourke, and H.M. Ajo, 2012. Summary of XRD and SEM Analysis of Tank 18 Samples. SRNL-L3100-2012-00017, Savannah River National Laboratory, Aiken, SC.

Hobbs, D.T., 2012. Form and Aging of Plutonium in Savannah River Site Waste Tank 18. SRNL-STI-2012-00106, Savannah River National Laboratory, Aiken, SC.

Höglund, L.O., 2001. Project SAFE: Modelling of long-term concrete degradation processes in the Swedish SFR repository. SKB Report R-01-08, Swedish Nuclear Fuel and Waste management Co., Stockholm, Seden.

Hower, J.C., R.F. Rathbone, J.D. Robertson, G. Peterson, and A.S. Trimble, 1999. Petrology, mineralogy, and chemistry of magnetically-separated sized fly ash. *Fuel*, 78, 197-203.

Hummel, W., U. Berner, E. Curti, F.J. Pearson, and T. Thoenen, 2002. "Nagra/PSI Chemical Thermodynamic Data Base 01/01." Techical Report 02-16, National Cooperative for the Disposal of Radioactive Waste.

Kaplan, D.I., T. Hang, and S. Aleman, 2005. Estimated Duration of the Reduction Capacity within a High Level Waste Tank (U), WSRC-RP-2005-01674, Washington Savannah River Company, Aiken, SC.

Krupa, K.M., and R.J. Serne, 1998. Effects on Radionuclide Concentrations by Cement/Ground-Water Interactions in Support of Performance Assessment of Low-Level Radioactive Disposal Facilities. NUREG/CR-6377 (PNNL-11408), Nuclear Regulatory Commission.

Kulik, D.A., 2006. "Improving the structural consistency of C-S-H solid solution thermodynamic Lothenbach, B., and F. Winnefeld. "Thermodynamic modelling of the hydration of Portland cement." *Cement and Concrete Research*, 36, 209-226.

Langmuir, D., 1997. Aqueous Environmental Geochemistry. Prentice Hall, Upper Saddle River, NJ.

Langton, C.A., 2009. Saltstone Matrix Characterization and Stadium Simulation Results: SIMCO Technologies, Inc. Task 6 Report. SRNL-STI-2009-00477, Rev. 0. Savannah River National Laboratory, Aiken, SC.

Langton, C.A., 2010. Chemical Degradation Assessment for the H-Area Tank Farm Concrete Tanks and Fill Grouts. SRNL-STI-2010-00035, Rev. 0, Savannah River National Laboratory, Aiken, SC.

Lemire, R.J., J. Fuger, H. Nitsche, P. Potter, M.H. Rand, J. Rydberg, K. Spahui, J.C. Sullivan, W.J. Ullman, P. Vitorge, and H. Wanner, 2001. Chemical Thermodynamics of Neptunium and Plutonium. North-Holland, Amsterdam.

Lothenbach, B. and F. Winnefeld, 2006. Thermodynamic modeling of the hydration of Portland cement. *Cement and Concrete Research*, 36, 209-226.

Lozano, J.C., F. Fernandez, and J.M.G. Gomez, 1997. Preparation of alpha-spectrometric sources by coprecipitation with Fe(OH)3: Application to actinides. *Applied Radiation and Isotopes.*, 48, 383-389.

Millings, M., J. Noonkester, and L. Bagwell, 2012. Summary Dissolved Oxygen in Water Table Wells at SRS. SRNL-L3200-2011-00011, Savannah River National Laboratory, Aiken, SC.

Oji, L.N., D. Diprete, and C.J. Coleman, 2010. Charaterization of Additional Tank 18F Samples. SRNL-STI-2010-00386, Rev. 0., Savannah River National Laboratory, Aiken, SC.

Oji, L.N., D. Diprete, and D.R., D.R. Click, 2009. Characterization of the Tank 18F Samples. SRNL-STI-2009-00625, Rev. 0.

Roberts, K.A. and D.I. Kaplan, 2009. Reduction Capacity of Saltstone and Saltstone Components. SRNL-STI-2009-00637, Savannah River National Laboratory, Aiken, SC.

Roine, A., 2009. HSC Chemistry® Version 7.0 User's Guide, Volume 1/2 Chemical Reaction and Equilibrium Software with Extensive Thermochemical Database and Flowsheet Simulation. 09006-ORC-J, Outotec Research Oy, Finland.

Slater, S.A., D.B. Chamberalin, A.A. Aase, B.D. Babcock, C.Conner, J. Sedlet, and G.F. Vandegrift, 1997. Optimization of magnetite carrier precipitation process for plutonium waste reduction. *Separation Science and Technology*, 32, 127-147.

Stefanko, D.B. and C.A. Langton, 2011. Tanks 18 and 19-F Structural Flowable Grout Fill Material Evaluation and Recommendations. SRNL-STI-2011-00551, Savannah River National Laboratory, Aiken, SC.

Strom, R.N. and D.S. Kaback, 1992. Groundwater Geochemistry of the Savannah River Site and Vicinity (U). WSRC-RP-92-450, Westinghouse Savannah River Company, Aiken SC.

Appendix 1 – List of Minerals Considered in Grout Simulations and Their Chemical Formulas

Mineral	**Chemical Formula**
Brucite	$Mg(OH)_2$
C4AH13	$Ca_4Al_2O_7 \cdot 13H_2O$
Calcite	$CaCO_3$
Ettringite	$Ca_6Al_2(SO_4)_3(OH)_{12} \cdot 26H_2O$
$Fe(OH)_{3(am)}$	$Fe(OH)_{3(am)}$
Fe-Ettringite	$Ca_6Fe_2(SO_4)_3(OH)_{12} \cdot 26H_2O$
Gibbsite	$Al(OH)_3$
Gypsum	$CaSO_4 \cdot 2H_2O$
JenD	$Ca_{1.5}Si_{0.67}O_{2.84} \cdot 2.5H_2O$
JenH	$Ca_{1.33}Si_{1.0}O_{3.33} \cdot 2.17H_2O$
Maghemite	Fe_2O_3
Magnetite	Fe_3O4
Monocarboaluminate	$Ca_4Al_2O_6(CO_3) \cdot 11H_2O$
OH-Hydrotalcite	$Mg_4Al_2(OH)_{14} \cdot 3H_2O$
Portlandite	$Ca(OH)_2$
Amorphous Silica	SiO_2
TobD	$Ca_{0.88}Si_{0.67}O_{2.22} \cdot 1.83H_2O$
TobH	$Ca_{0.66}Si_2O_{4.66} \cdot 1.5H_2O$

Appendix 2 – Thermodynamic Data and Sources Entered into PHREEQC Database

Reaction	Log K	Ref.
Cementitious Minerals		
$Ettringite + 12H^{+} = 6Ca^{+2} + 2Al^{+3} + 3SO_4^{-2} + 38H_2O$	56.67	a
$Fe\text{-}Ettringite + 12H^{+} = 6Ca^{+2} + 2Fe^{+3} + 3SO_4^{-2} + 38H_2O$	49.79	a
$JenH + 2.66H^{+} = 1.33Ca^{+2} + Si(OH)_{4(aq)} + 1.5H_2O$	22.10	b
$JenD + 3H^{+} = 1.5Ca^{+2} + 0.67Si(OH)_{4(aq)} + 2.66H_2O$	28.72	b
$TobH + 1.32H^{+} + 1.84H_2O = 0.66Ca^{+2} + 2Si(OH)_{4(aq)}$	5.42	b
$Portlandite + 2H^{+} = Ca^{+2} + 2H_2O$	22.80	b
$Calcite = Ca^{+2} + CO_3^{-2}$	-9.59	a
$TobD + 1.66H^{+} = 0.83Ca^{+2} + 0.67Si(OH)_{4(aq)} + 1.32H2O$	13.56	a
$OH\text{-}Hydrotalcite + 14H^{+} = 4Mg^{+2} + 2Al^{+3} + 17H_2O$	73.74	a
$Brucite + 2H^{+} = Mg^{+2} + 2H_2O$	16.84	a
$Monocarboaluminate + 12H^{+} = 4Ca^{+2} + 2Al^{+3} + CO_3^{-2} + 17H_2O$	70.29	a
$C4AH13 + 14H^{+} = 4Ca^{+2} + 2Al^{+3} + 20H_2O$	104.20	a
$Gibbsite + 3H^{+} = Al^{+3} + 3H_2O$	7.76	a
$Silica(am) + 2H_2O = Si(OH)_{4(aq)}$	-2.71	a
$Maghemite + 6H^{+} = 2Fe^{+3} + 3H_2O$	2.54	c
$Magnetite + 8H^{+} = Fe^{+2} + 2Fe^{+3} + 4H_2O$	10.13	d
$Pyrite + H_2O = Fe^{+2} + 2HS^{-} + 0.5O_{2(aq)}$	-60.53	d
Plutonium Solid Phases		
$PuO_{2(am,hyd)} + 4H^{+} = Pu^{+4} + 2H_2O$	-1.99	e
$PuO_{2(c)} = Pu^{+4} + 2H_2O$	-8.03	e
$Pu(OH)_2CO_{3(s)} + 2H^{+} = Pu^{+4} + CO_3^{-2} + 2H_2O$	-25	d
Plutonium Aqueous Species		
$Pu^{+3} + 0.25O_{2(aq)} + H^{+} = Pu^{+4} + 0.5H_2O$	3.80	e
$PuO_2^{+} + 3H^{+} = Pu^{+4} + 0.25O_{2(aq)} + 1.5H_2O$	-4.04	e
$PuO_2^{+2} + 2H^{+} = Pu^{+4} + 0.5O_{2(aq)} + H_2O$	-9.71	e
$PuOH^{+2} + H^{+} = Pu^{+3} + H_2O$	6.90	e
$PuOH^{+3} + H^{+} = Pu^{+4} + H_2O$	-0.60	e
$Pu(OH)_2^{+2} + 2H^{+} = Pu^{+4} + 2H_2O$	-0.60	e
$Pu(OH)_3^{+} + 3H^{+} = Pu^{+4} + 3H_2O$	2.30	e
$PuO2(OH)_{(aq)} + H^{+} = PuO_2^{+} + H_2O$	9.73	e
$PuO2(OH)^{+} + H^{+} = PuO_2^{+2} + 2H_2O$	5.50	e
$PuO2(OH)_{2(aq)} + 2H^{+} = PuO_2^{+2} + 2H_2O$	13.20	e
$Pu(OH)_{4(aq)} + 4H^{+} = Pu^{+4} + 4H_2O$	8.50	e
$PuO_2CO_{3(aq)} + H^{+} = PuO_2^{+2} + CO_3^{-2}$	-9.50	e
$PuO_2CO_3^{-} = PuO_2^{+2} + CO_3^{-2}$	-5.12	e
$PuO_2(CO_3)_2^{-2} = PuO_2^{+2} + 2CO_3^{-2}$	-14.70	e
$PuO_2(CO_3)_3^{-4} = PuO_2^{+2} + 3CO_3^{-2}$	-18.00	e
$PuO_2(CO_3)_3^{-5} = PuO_2^{+} + 3CO_3^{-2}$	-5.03	e
$Pu(CO_3)_4^{-4} = Pu^{+4} + 4CO_3^{-2}$	-37.00	e
$Pu(CO_3)_5^{-6} = Pu^{+4} + 5CO_3^{-2}$	-35.65	
Miscellaneous Aqueous Species		
$CO_{2(aq)} + H_2O = CO_3^{-2} + 2H^{+}$	-16.68	e
$HCO_3^{-} = CO_3^{-2} + H^{+}$	-10.33	e

$CaH_2SiO_{4(aq)} + 2H^+ = Ca^{+2} + Si(OH)_{4(aq)}$	18.54	a
$CaH_3SiO_4^+ + H^+ = Ca^{+2} + Si(OH)_{4(aq)}$	8.64	a
$MgH_2SiO_{2(aq)} + 2H^+ = Mg^{+2} + Si(OH)_{4(aq)}$	17.44	a
$MgH_3Si(OH)_{4(aq)} + H^+ = Mg^{+2} + Si(OH)_{4(aq)}$	8.31	a
$AlSiO(OH)_3^{+2} + H^+ = Al^{+3} + Si(OH)_{4(aq)}$	2.41	a
$AlSiO(OH)_6^- + 4H^+ = Al^{+3} + Si(OH)_{4(aq)} + 3H_2O$	19.28	a
$FeSiO(OH)_3^{+2} + H^+ = Fe^{+3} + Si(OH)_{4(aq)}$	0.11	a

a—Lothenbach and Winnefeld (2006)

b—Kulik (2011)

c—Roine (2009)

d—HATCHES v. NEA18

e—Nuclear Energy Agency (2005)

Summary of Sources of Thermodynamic Data

Lothenbach and Winnefeld (2006) -- The thermodynamic data relating to cementitious solids and associated aqueous species comes predominantly from the default database of the PSI-GEMS software:

Hummel, W. U. Berner, E.Curti, F.J. Pearson, and T.Thoenen, 2002. Nagra/PSI Chemical Thermodynamic Database 01/01. Nagra Technical Report NTB 02-16, Nagra, Wettingen, Switzerland.

This is a traceable, quality assured database from the Paul Scherrer Institute (PSI). The thermodynamic data used by Lothenbach and Winnefeld (2006) for the solid phases gypsum and C4AH13 and the aqueous species $CaSO_4^o$ come from other traceable sources.

Kulik (2011) -- A revision of the thermodynamic solid solution model for C-S-H to make it consistent with structural observations. An earlier model with associated thermodynamic data developed by Kulik was used in the PSI-GEMS databse used by Lothenbach and Winnefeld (2006). The newer thermodynamic data developed in Kulik (2011) was used in the current report to account for the C-S-H solid solution.

Roine (2009) -- Presents the commercially available chemical processing software HSC version 7.0. The extensive thermochemical database that is part of this software package is fully traceable with most sources from widely accepted compilations of thermochemical data.

HATCHES Version NEA18 -- HATCHES is the acronym for **HA**rwell/Nirex **T**hermochemical Database for **CH**emical **E**quilibrium **S**tudies. The database is fully traceable, quality assured product of Serco

Assurance prepared for Nirex. Nirex was an organization created by the United Kingdom to study safe geological disposal of radioactive waste. It's functions have now been incorporated into the National Disposal Authority (NDA). The original databse was described in:

Bond, K.A., T.G. Heath, and C.J. Tweed, 1997. HATCHES: A Referenced Thermodynamic Database for Chemical Equilibirum Studies. Nirex Report NSS/R379.

The latest version can be downloaded from: http://www.sercoassurance.com/hatches/

Nuclear Energy Agency (NEA) Database -- A product of the Nuclear Energy Agency Thermochemical Database Project. The database is " comprehensive, internally consistent, internationally recognized and quality assured". Downloads containing thermochemical data for inorganic compounds and aqueous complexes for various elements of interest to radioactive waste disposal are available from: http://www.oecd-nea.org/dbtdb/.